A fast, analytically-based method to optimize local transmit efficiency for a transmit array

[1]Giuseppe Carluccio, [1]Christopher M. Collins, [2]Danilo Erricolo

[1]Department of Radiology, New York University, New York, NY 10016
[2]Department of Electrical and Computer Engineering, University of Illinois at Chicago, Chicago, IL 60607

Running Title: Optimizing local B1+ efficiency with transmit array

Corresponding Author:

Danilo Erricolo, PhD

Professor of Electrical and Computer Engineering

University of Illinois at Chicago

851 S. Morgan M/C 154

Chicago, IL. 60607

Phone: 312.996.5771

FAX: 312.996.6465

erricolo@ece.uic.edu

Words count: 2786

Abstract

Purpose: to develop an analytically-based algorithm for rapid optimization of the local RF magnetic (B_1^+) field intensity for a given RF power through a transmit array. The analytical nature of the method will yield insight to optimization requirements and provides a valuable reference for numerically-based searches.

Materials and Methods: with knowledge of the B_1^+ field distribution generated by each single coil of the array, both the phases and the amplitudes of each coil current are optimized to maximize the magnitude of the B_1^+ field in a specific location of the body per unit of power transmitted through the array and, consequently, minimizing the whole body SAR for a given pulse sequence.

Results: simulations considering the human body show that the proposed method can reduce the whole body SAR for a given B1+ magnitude at the location of interest by a factor of about 6.3 compared to the classic birdcage current configuration, and by a factor of 3.2 compared to phase-only shimming in a case with significant coupling between the elements of the array.

Conclusion: the proposed method can rapidly provide valuable information pertinent to the optimization of field distributions from transmit arrays.

Keywords: radiofrequency, MRI, shimming, power, SAR, spectroscopy

Introduction

A current challenge for high field MRI is non-uniformity of the radiofrequency magnetic excitation field (B_1^+). Because the frequency of the B_1^+ field is proportional to the strength of the static magnetic (B_0) field, at high B_0 fields the B_1^+ field has a relatively short wavelength, resulting in non-homogeneous flip-angle distributions and ultimately affecting the quality of the final images. RF shimming is the simplest of a variety of approaches using an array of coils in transmission to address this challenge. In RF shimming, a more desirable RF electromagnetic field distribution is achieved with adjustment of the magnitude and/or phase of the currents or voltages driving the elements of the transmit array (1-3). More advanced methods can achieve excitation distributions very different than the RF field distributions (4-6), but in general require significantly longer pulse durations and/or greater total RF energy to achieve a given average flip angle.

In some cases, especially in the human head, it can be possible to achieve reasonably homogeneous excitation of almost the entire sample volume with use of RF shimming (7). In other cases, however, it may not be possible or advantageous to optimize field homogeneity over a large volume. If we are either interested only in a single small volume, such as in spectroscopy (8), or in imaging where the region of interest (ROI) is small compared to the sample volume and the sample is large enough that RF shimming cannot readily produce a homogeneous field across its volume (9), local RF shimming may be preferred. In these cases, it is expected that the B_{1^+} field across an ROI smaller than about one quarter wavelength will be fairly homogeneous as long as there is constructive interference from the fields of individual arrays there, and attention can be devoted to the efficiency with which B_{1^+} is produced in the smaller ROI.

By reducing the amount of power required to create a given B_1^+ field in the region of interest, the whole-body (global) specific absorption rate (SAR) is reduced, and there is greater flexibility in the imaging parameters (including imaging time) that can be used. It has been observed that limits on local SAR can often be exceeded before those on average SAR will (10). According to the most recent version of widely-used guidelines (11), when an array of transmit coils is used as a volume coil there is no limit on local SAR, providing another motivation for considering whole body SAR. It is also notable that average SAR is more readily monitored than local SAR (12), making methods to reduce it more amenable to verification in regular use. Even in cases where local SAR may be the limiting factor, however, rapidly-determined shim values that produce optimal overall efficiency and minimal whole-body SAR can provide a valuable reference for other optimization methods designed to consider local SAR.

Although a number of papers have focused on controlling local or average SAR in RF shimming of a large region (13) or in advanced transmit array pulse designs for homogeneous excitation (14), comparatively little work has considered RF shimming on a localized region. Methods for local RF shimming designed to minimize power requirements and whole-body average SAR have included an analytically-based approach to adjusting only the phase of array elements for imaging of the human prostate *in vivo* (9), an approach based on the Rayleigh quotient optimization (15, 16)and a numerical optimization of the phase and magnitude of all elements in simulation-based demonstrations considering models of the human body (17).

Here we present a simple, analytically-based method to adjust both magnitude and phase of all elements for local RF shimming to minimize power requirements and whole-body SAR.

Materials and Methods

One application of a method that optimizes only the phases of the transmit array elements was shown previously for application to the prostate (9). Indicating with $B_{1,i,m}^{+}$ the circularly polarized component of the B_1 field generated by the *i*-th element of the transmit array in the m-th voxel of the ROI when the *i*-th element is driven with the reference current $I_{i,ref}$, this phase optimization process consists of acquiring the phases of all $B_{1,i,m}^{+}$ fields in the M voxels belonging to the ROI with a technique of B_1 phase mapping, and adjusting the phase of the input to the *i*-th element by an amount equal to the opposite of the measured phase of $B_{1,i,m}^{+}$ fields in the ROI. The resulting optimal coil current could be written

$$I_i = I_{i,ref}\, e^{-j\frac{1}{M}\sum_{m=1}^{M} \angle\, B_{1,i,m}^{+}} \;, \qquad\qquad [1]$$

where *j* is the imaginary unit. After this, all the B_1^{+} fields generated by each element of the array will add constructively in the ROI, producing B_1^{+} much more efficiently than if destructive interference were to occur there. Note that it must be possible to control the current in each element as in Eq. [1] to provide the desired effect on the phase of the field produced.

In the following, we propose and demonstrate a simple method to find the set of currents I_i having both optimal phase and optimal amplitude. This method is developed with the assumption that complex current in each element is known explicitly. In some configurations of transmit arrays, this is indeed the case (18). In others, with adequate measurement of the impedance matrix and knowledge of the input voltage it is technically possible to determine the

currents. In any case, this work will provide an intuitive understanding of the requirements for optimizing the efficiency of a transmit array for local excitation.

In the case that $I_{i,ref}$ is identical for all the elements and equal to I_{ref}, we can write the desired current driving each element of the transmit array as

$$I_i = I_{ref} C A_i e^{-j\angle\frac{1}{M}\sum_{m=1}^{M} B_{1,i,m}^+} . \quad\quad [2]$$

where the optimal current amplitudes A_i are dimensionless real positive numbers, and C is a normalization factor equal for all the elements of the transmit array. The value for C can be used to normalize the currents to satisfy, if necessary, some safety requirements such as local average SAR, temperature increase, or to obtain a specific value of flip-angle while still keeping the same efficiency in terms of transmitted field B_1^+ and generated power. Both the magnitudes and phases of B_1^+ can be determined experimentally (8, 19). The amplitudes A_i are determined through the optimization of a cost function that attempts to simultaneously maximize the total B_1^+ field at the desired ROI and minimize the transmitted power, while the phases are determined as done in equation [2].

The power transmitted through an array can be calculated as

$$P_{Tx} = \frac{1}{2} \sum_{k=1}^{N} \sum_{i=1}^{N} Re\{I_i Z_{ik} I_k^*\}, \quad\quad [3]$$

where Z_{ik} are the elements of the impedance matrix $\mathbf{Z}$ and represent the mutual impedance between the *i-th* and the *k-th* element of the array, which can be measured with a network analyzer.

The cost function depends on the observables to be optimized. In particular, in this work we choose to minimize the square root of the transmitted power over the average B_1^+ field in the ROI:

$$f = \frac{\sqrt{P_{Tx}}}{\left|\frac{1}{M} \sum_{m=1}^{M} B_{1,m}^+\right|}, \qu\quad [4]$$

where $B_{1,m}^+ = \sum_{i=1}^{N} A_i B_{1,i,m}^+$. This will be at a minimum when P_{Tx} is minimized for a given B_1^+ amplitude. There are two motivations to minimize P_{Tx}: 1) the generated power provides an upper bound to the whole-body SAR and 2) P_{Tx} is a measurable parameter in an MRI system. However, if additional information is available through a more accurate relation between the generated power and the SAR (12), the cost function could be modified to also take advantage of this. The definition of the function f contains the square root of the generated power in order to avoid a linear dependence with the currents that generate the fields. To clarify the explanation of our method, we

consider two different cases. In the first one, we examine a simplified situation where there is negligible coupling among the array elements, which causes the impedance matrix **Z** to be diagonal, and an exact analytical solution is obtained. In the second case, the more general situation of non-negligible coupling among array elements is examined and it is solved through a diagonalization of the impedance matrix **Z**. Keeping these two cases separate allows for evaluation of two different cases (decoupled and coupled arrays) in a natural progression.

Case 1: negligible mutual coupling. When the coupling between different elements of the array is small ($|Z_{ik}| \ll |Z_{ii}|$ for all i and all $k \neq i$) the values of the amplitudes that minimize f can be obtained by finding a set of currents that cause the gradient of f to be zero. Specifically, the generated power is approximated as

$$P_{Tx} \approx \frac{1}{2} \sum_{i=1}^{N} Re\{Z_{ii}\}|I_i|^2 = \frac{1}{2} C^2 \sum_{i=1}^{N} Re\{Z_{ii}\}A_i^2. \qquad [5]$$

and the components of the first derivative are set to zero, yielding

$$\frac{\partial f}{\partial A_i} = \frac{\partial \left(\frac{\sqrt{\frac{1}{2}C^2 \sum_{i=1}^{N} Re\{Z_{ii}\}A_i^2}}{\sum_{i=1}^{N} CA_i \left|\frac{1}{M}\sum_{m=1}^{M} B_{1,i,m}^+\right|} \right)}{\partial A_i} = \sqrt{\frac{1}{2}} \frac{\partial \left(\frac{\sqrt{\sum_{i=1}^{N} Re\{Z_{ii}\}A_i^2}}{\sum_{i=1}^{N} A_i \left|\frac{1}{M}\sum_{m=1}^{M} B_{1,i,m}^+\right|} \right)}{\partial A_i} = 0 \qquad [6]$$

or equivalently

$$\frac{\partial f}{\partial A_i} = \sqrt{\frac{1}{2}} \left[\frac{Re\{Z_{ii}\}A_i \sum_{l=1}^{N} A_l \left|\frac{1}{M}\sum_{m=1}^{M} B_{1,l,m}^+\right| - \left|\frac{1}{M}\sum_{m=1}^{M} B_{1,i,m}^+\right| \sum_{l=1}^{N} Re\{Z_{ll}\}A_l^2}{\sqrt{\sum_{i=1}^{N} Re\{Z_{ii}\}A_i^2} \left(\sum_{i=1}^{N} A_i \left|\frac{1}{M}\sum_{m=1}^{M} B_{1,i,m}^+\right|\right)^2} \right] = 0 \qquad [7]$$

By solving eq. [7] for A_i

$$A_i = \frac{\left|\frac{1}{M}\sum_{m=1}^{M} B_{1,i,m}^+\right|}{Re\{Z_{ii}\}} \frac{\sum_{l=1,l\neq i}^{N} Re\{Z_{ll}\}A_l^2}{\sum_{l=1,l\neq i}^{N} \left|\frac{1}{M}\sum_{m=1}^{M} B_{1,l,m}^+\right|A_l} \qquad [8]$$

and assuming $A_l = \rho \frac{\left|\frac{1}{M}\sum_{m=1}^{M} B_{1,l,m}^+\right|}{Re\{Z_{ll}\}}$, where $\rho = 1\frac{\Omega}{T}$ is introduced to keep the terms A_l dimensionless, the

ratio $\frac{\sum_{l=1,l\neq i}^{N} Re\{Z_{ll}\}A_l^2}{\sum_{l=1,l\neq i}^{N} \left|\frac{1}{M}\sum_{m=1}^{M} B_{1,l,m}^+\right|A_l}$ becomes equal to ρ . Hence, the terms A_i are also given by

$$A_i = \rho \frac{\left|\frac{1}{M}\sum_{m=1}^{M} B_{1,i,m}^+\right|}{Re\{Z_{ii}\}} \qquad [9]$$

which corresponds to the solution of eq. [7].

Therefore, from the measurements of $B_{1,i}^+$ in the ROI and Z_{ii}, the optimal amplitudes A_i that minimize the cost function f at the ROI can be determined immediately. If a value for C that brings B_1^+ back to its original strength is added, a physical interpretation of this solution is seen when

observing that its effect is to increase the driving current of the elements that contribute to the average B_1^+ field amplitude at the ROI most efficiently and reduce the driving current of the elements that do so least efficiently.

Case 2: non-negligible coupling. If the coupling among the elements of the array is significant, the impedance matrix $\mathbf{Z}$ is not diagonal as in Case 1 and linear algebra operations can be used to solve an equation similar to eq. [7] of Case 1.

Let $\mathbf{A}$ be the currents vector composed of the coefficients A_i, and $\mathbf{B_1^+}$ the vector containing the average values of the circularly polarized field B_1 generated by each element of the array at the location of interest. Then, we can rewrite eq. [4] as

$$f = \frac{\sqrt{\frac{1}{2} Re\{\mathbf{A^{*T} Z A}\}}}{\left|\mathbf{B_1^{+T} A}\right|} \qquad [10]$$

where the i-th element of the vector $\mathbf{B_1^+}$ is equal to $B_{1,i}^+ = \frac{1}{M}\sum_{m=1}^{M} B_{1,i,m}^+$ and where the superscripts $*$ and T indicate the complex conjugate and transpose operators, respectively.

Let us write

$$\mathbf{Z} = \mathbf{Z_R} + j\mathbf{Z_I} \qquad [11]$$

where

$$\mathbf{Z_R} = Re\{\mathbf{Z}\} \qquad [12]$$

and

$$\mathbf{Z_I} = Im\{\mathbf{Z}\} \qquad [13]$$

With the definitions in eq. [12]-[13], we can rewrite eq. [10] as

$$f = \frac{\sqrt{\frac{1}{2} Re\{\mathbf{A^{*T} Z_R A} + j\,\mathbf{A^{*T} Z_I A}\}}}{\left|\mathbf{B_1^{+T} A}\right|} = \frac{\sqrt{\frac{1}{2} Re\{\mathbf{A^{*T} Z_R A}\} + \frac{1}{2} Re\{j\,\mathbf{A^{*T} Z_I A}\}}}{\left|\mathbf{B_1^{+T} A}\right|} \qquad [14]$$

We can decompose both the matrices Z_R and Z_I through the use of the eigenvector matrices Q_R and Q_I

$$Z_R = Q_R^{-1} D_R Q_R \qquad\qquad [15]$$

$$Z_I = Q_I^{-1} D_I Q_I \qquad\qquad [16]$$

where D_R and D_I are diagonal matrices containing the eigenvalues of the matrices Z_R and Z_I.

Since Z is symmetric, Z_R and Z_I are symmetric too, and since both Z_R and Z_I have all real elements, $Q_R^{-1} = Q_R^{*T}$ and $Q_I^{-1} = Q_I^{*T}$. Thus,

$$f = \frac{\sqrt{\frac{1}{2} Re\left\{A^{*T} Z_R\, A\right\} + \frac{1}{2} Re\left\{j\, A^{*T} Z_I\, A\right\}}}{\left|B_1^{+T} A\right|} = \frac{\sqrt{\frac{1}{2} Re\{A^{*T} Q_R^{*T} D_R Q_R\, A\} + \frac{1}{2} Re\{j\, A^{*T} Q_I^{*T} D_I Q_I\, A\}}}{\left|B_1^{+T} A\right|} \quad [17]$$

We can write $A^{*T} Q_R^{*T} = (Q_R\, A)^{*T}$ and $A^{*T} Q_I^{*T} = (Q_I\, A)^{*T}$

$$f = \frac{\sqrt{\frac{1}{2} Re\{(Q_R\, A)^{*T} D_R (Q_R\, A)\} + \frac{1}{2} Re\{j\, (Q_I\, A)^{*T} D_I (Q_I\, A)\}}}{\left|B_1^{+T} A\right|} = \frac{\sqrt{\frac{1}{2} Re\{(Q_R\, A)^{*T} D_R (Q_R\, A)\}}}{\left|B_1^{+T} A\right|} \quad [18]$$

because the product $(Q_I\, A)^{*T} D_I (Q_I\, A)$ in eq. [17] is real since it is a quadratic form and the eigenvalues of D_I are real. Thus, $j(Q_I\, A)^{*T} D_I (Q_I\, A)$ is purely imaginary, and $Re\{j(Q_I\, A)^{*T} D_I (Q_I\, A)\}$ is null.

We can rewrite the denominator of eq. [18]

$$\left|B_1^{+T} A\right| = \left|B_1^{+T} I A\right| \qquad\qquad [19]$$

where I is the identity matrix. By definition of the inverse of a matrix

$$\left| B_1^{+^T} I A \right| = \left| B_1^{+^T} Q_R^{-1} Q_R A \right| \tag{20}$$

By defining $E = Q_R A$ and $F = B_1^{+^T} Q_R^{-1}$, we have

$$f = \frac{\sqrt{\frac{1}{2} Re\{E^{*T} D_R E\}}}{|FE|} \tag{21}$$

The minimization of eq. [21] is equivalent to that of Case 1, provided that the following substitutions are made. The vector E is the unknown, the impedance matrix is D_R (that is equivalent to an impedance matrix with no coupling since D_R is a diagonal matrix), and F is the magnetic field vector. With these substitutions, eq. [9] is used to find the values of E that minimize eq. [21].

After E is obtained, the final current vector A is computed as

$$A = Q_R^{-1} E \tag{22}$$

Method

The performance of the proposed algorithm for non-negligible coupling was compared with two other methods to compute the coil currents: 1) the distribution for a birdcage coil in ideal mode 1 resonance and 2) a phase-only optimization published previously (9). Comparisons included examinations of the magnitude of the B_1^+ field in the ROI for a given P_{Tx}, and also of the P_{Tx} required to produce a given B_1^+ for both the negligible and the non negligible coupling cases. In all cases, the field distributions were computed numerically at 300 MHz for a body-sized 8-element array of stripline elements spaced equidistantly on the surface of a cylinder within a large cylindrical shield and loaded with a human body model (20) positioned with its heart near the center of the array (Fig. 1). The field distribution for each element of the array was computed with all other elements present, but with open circuit at each end to simulate a case of minimal coupling between elements,

since coupling between the elements and their fields can be added later. All numerical simulations were performed using a commercially available full-wave electromagnetic field simulator (XFDTD; Remcom, Inc.; State College, PA; USA) and with I_{ref} of 1 Ampere. In the comparisons, the optimized coil currents were normalized by changing the value of the factor C in Eq. 2 so that either P_{Tx} or B_{1^+} (as desired) in the ROI was the same for all three cases. For the uncoupled case, fields were used as computed with each element driven individually and as if the coupling matrix was the identity matrix. For the case study with significant coupling two appendages were applied at the extremities of each stripline, which more easily induce fields among the elements of the array. The structure of the impedance matrices of both the negligible coupling and non negligible coupling cases used in this study is reported in Fig. 2. Hence, it should be clear that this method could be applied to an experimentally measured impedance matrix. The comparisons were performed considering a cubic ROI 5mm on each side placed both in the heart (centrally located) and in the shoulder (peripherally located).

Results

Table 1 gives the magnitude of B_1^+ for each target ROI in each of three current distributions normalized to produce a whole-body average SAR of 2 W/Kg with negligible coupling between array elements. Table 2 presents the same for the case with significant coupling. Figure 3 reports for the two ROIs, for each element of the array having negligible mutual coupling, the values of the real part of the self-impedance $Re\{Z_{ii}\}$, the average absolute value of the circularly polarized magnetic field in the two ROI, the amplitude of the currents obtained by applying eq. [9] scaled by the factor C to produce the fields shown in Table 1. Figures 4 and 5 show $|B_1^+|$ field distributions obtained in the cross section containing the two different ROIs for the two different cases. For an ROI in the heart and given P_{Tx}, the proposed algorithm for optimizing transmit efficiency considering both amplitude and phase of each current element produces an average B_1^+ field having amplitude 5.39 times larger than that of the birdcage coil and 1.20 times larger than that of the phase-only optimization. For an ROI in the shoulder and given P_{Tx}, the proposed algorithm produces a B_1^+ field having amplitude 2.22 times larger than that of the birdcage coil and 1.70 times larger than that of the phase-only optimization.

With the elements of the array having non negligible coupling among them Table 1 gives the B_1^+ for each target ROI in each of three current distributions normalized to produce the same P_{Tx}.

For an ROI near the heart, the proposed algorithm for optimizing transmit efficiency considering both amplitude and phase of each current element produces a B_1^+ field having amplitude 4.73 times larger than that of the birdcage coil and 1.19 times larger than that of the phase-only optimization. For an ROI in the arm, the proposed algorithm produces a B_1^+ field having amplitude 2.57 times larger than that of the birdcage coil and 2.00 times larger than that of the phase-only optimization.

Using these same numbers it is also possible to determine the power required to produce a given B_{1^+} in each case. To produce a given B_{1^+} in an ROI near the heart, the proposed algorithm will require 0.034 times the power required by a birdcage coil and 0.694 times the power required by the phase-only optimization for the case of negligible coupling among the elements of the array, while it will require 0.045 times the power required by a birdcage coil and 0.706 times the power required by the phase-only optimization for the case of non negligible coupling among the elements of the array. To produce a given B_{1^+} in an ROI in the shoulder, the proposed algorithm will require 0.203 times the power required by a birdcage coil and 0.346 times the power required by the phase-only optimization for the case of negligible coupling, while it will require 0.151 times the power required by a birdcage coil and 0.25 times the power required by the phase-only optimization for the non negligible coupling. For a given pulse sequence this would translate to approximately one-fifth the whole-body SAR in the birdcage coil and one third of that in the phase-only optimization.

Discussion

We have presented a simple, analytically-based method for optimizing transmit efficiency of exciting a local region considering both magnitude and phase of all elements in a transmit array. For a small ROI our method provides results that differ by only a few percent from the results obtained with the method in (15, 16) developed in parallel with our method (21). One advantage of our derivation is that it provides a more explicit relationship between the optimum values of the current amplitudes and the impedances and field distributions of the elements. . This is clearly evident in Figure 3 for the array having negligible coupling among the elements. Figure 3 shows also the relationship between impedances, the optimal amplitudes of the currents, and the values of the fields generated by the elements of the array. As in Eq. [9], the optimal current amplitude for each element is proportional to the ratio of the B_1 field it produces in the ROI to its impedance. In

the case of exciting a central location, this results in low optimal currents in elements near the arms, which have both relatively high impedance and relatively low B_1^+ in the ROI. When the ROI is in a peripheral location, however, the highest optimal current amplitudes are in the elements near the ROI due to the very low relative B_1^+ fields produced there by elements further away.

In regions near the center of the torso this method is seen to perform slightly better than a previously published analytically-based phase-only optimization (9). Away from the center of the array and sample the improvement over the phase-only optimization is more dramatic. This is to be expected because, as some elements far from the center of the array are likely to transmit much more efficiently than others, increasing the value of magnitude-and-phase optimization. Finally, it is interesting to note that when the coupling among the elements of the array is significant the algorithm provides a set of phases different from the ones obtained by a method designed simply to produce constructive interference.

References

1. Hoult DI. The sensitivity and power deposition of the high field imaging experiment. J Magn Reson Imaging 2000;12:46–67.
2. Ibrahim TS, Lee R, Baertlein BA, Abduljalil AM, Zhu H, Robitaille PL. Effect of RF coil excitation on field inhomogeneity at ultra high fields: a field optimized TEM resonator. Magn Reson Imaging 2001; 19:1339–1347.
3. Vaughan JT, DelaBarre L, Snyder C, Tian J, Akgun C, Shrivastava D, Liu W, Olson C, Adriany G, Strupp J, Andersen P, Gopinath A, van de Moortele P-F, Garwood M, Ugurbil K. 9.4T Human MRI: preliminary results. Magn Reson Med 2006;56:1274–1282.
4. Katscher U, Bo¨rnert P, Leussler C, van den Brink JS. Transmit SENSE. Magn Reson Med 2003;49:144–150.
5. Zhu Y. Parallel excitation with an array of transmit coils. Magn Reson Med 2004;51:775-784.
6. Saekho S, Yip C-Y, Noll DC, Boada FE, Stenger VA. Fast-kz three-dimensional tailored radiofrequency pulse for reduced B1 inhomogeneity. Magn Reson Med 2006;55:719-724.
7. Mao W, Smith MB, Collins CM. Exploring the Limits of RF Shimming for High-Field MRI of the Human Head. Magn Reson Med 2006;56:918-922.
8. Versluis MJ, Kan HE, van Buchem MA, Webb AG. Improved Signal to Noise in Proton Spectroscopy of the Human Calf Muscle at 7 T Using Localized B_1 Calibration. Magn Reson Med 2010; 63: 207-211.
9. Metzger GJ, Snyder C, Akgun C, Vaughan T, Ugurbil K, Van de Moortele PF. Local B_1^+ shimming for prostate imaging with transceiver arrays at 7T based on subject-dependent transmit phase measurements. Magn Reson Med 2008;59:396–409.
10. Wang Z, Lin JC, Mao W, Liu W, Smith MB, and Collins CM. SAR and temperature: simulations and comparison to regulatory limits for MRI. J Magn Reson Imag 2007;26:437-441.
11. International Electrotechnical Commission. Medical electrical equipment – Part 2-33: particular requirements for the basic safety and essential performance of magnetic resonance equipment for diagnosis. IEC60601-2-33, edition 3.0. IEC Press, Geneva, 2010.
12. Zhu Y. In Vivo RF Power and SAR Calibration for Multi-Port RF Transmission. In: Proceedings of the International Society For Magn Reson Med, Honolulu, 2009, p. 2585.
13. Van den Berg CAT, van den Bergen B, Van de Kamer JB, Raaymakers BW, Kroeze H, Bartels LW, Lagendijk JJW. Simultaneous B_1^+ Homogenization and Specific Absorption Rate Hotspot Suppression Using a Magnetic Resonance Phased Array Transmit Coil. Magn Reson Med 2007; 57: 577-586.

14. Brunner DO and Pruessmann KP. Optimal design of multiple-channel RF pulses under strict power and SAR constraints. Magn Reson Med 2010;63:1280-1291.

15. Deniz CM, Brown R, Lattanzi R, Alon L, Sodickson DK, Zhu Y. Maximum efficiency RF shimming. Proceedings of the ISMRM 21st Annual Meeting, May 5-11 2012, Melbourne, p. 3479

16. Deniz CM, Brown R, Lattanzi R, Alon L, Sodickson DK, Zhu Y. Maximum efficiency RF shimming: Theory and Initial Application for Hip Imaging at 7 Tesla. Magn Reson Med 2012.

17. Abraham R, Ibrahim T. Proposed radiofrequency phased-array excitation scheme for homogenous and localized 7-tesla whole-body imaging based on full-wave numerical simulations. Magn Reson Med 2007;57:235-242.

18. Kurpad KN, Boskamp EB, Wright SM. Implementation of coil integrated RF power MOSFET as a voltage controlled current source in a transmit phased array coil. In: Proceedings of the 12th Annual Meeting of ISMRM, Kyoto, 2004, p. 1585.

19. Yarnykh VL. Actual Flip-Angle Imaging in the Pulsed Steady State: A Method for Rapid Three-Dimensional Mapping of the Transmitted Radiofrequency Field. Magn Reson Med 2007; 57:192-200.

20. Christ A, Kainz W, Hahn EG, Honegger K, Zefferer M, Neufeld E, Rascher W, Janka R, Bautz W, Chen J, Kiefer B, Schmitt P, Hollenbach H-P, Shen J, Oberle M, Szczerba D, Kam A, Guag JW, Kuster N. The virtual family – development of surface-based anatomical models of two adults and two children for dosimetric simulations.

21. Carluccio G, Collins CM, Erricolo D. An Analytical Method to Optimize Transmit Efficiency for Local Excitation with a Transmit Array. Proceedings of the ISMRM 21st Annual Meeting, May 5-11 2012, Melbourne, p. 2618

Table 1. Magnitude of the B_1^+ field produced by three different current distributions including optimizations for an ROI near the heart and in the shoulder for a transmit array having negligible coupling between its elements. In each case whole-body average SAR 2 W/Kg.

	$\frac{1}{M}\sum_{m=1}^{M}\left|B_{1,i,m}^+\right|$ for a ROI near heart (μT)	$\frac{1}{M}\sum_{m=1}^{M}\left|B_{1,i,m}^+\right|$ for a ROI near arm (μT)
Birdcage	0.4418	3.5181
Phase-only Optimization	1.9738	4.6195
Optimization with phase and amplitude	2.3800	7.8447

Table 2. Magnitude of the B_1^+ field produced by three different current distributions including optimizations for an ROI near the heart and in the shoulder for a transmit array having significant coupling between its elements. In each case whole-body average SAR 2 W/Kg.

	$\frac{1}{M}\sum_{m=1}^{M}\left|B_{1,i,m}^+\right|$ for a ROI near heart (μT)	$\frac{1}{M}\sum_{m=1}^{M}\left|B_{1,i,m}^+\right|$ for a ROI near arm (μT)
Birdcage	0.4147	3.3904
Phase-only Optimization	1.6458	4.3660
Optimization with phase and amplitude	1.9617	8.7185

Figure Caption

Figure 1: Geometry of the model used in simulations: a body-sized 8-element array of stripline elements spaced equidistantly on the surface of a cylinder within a large cylindrical shield and loaded with a human body model positioned with its heart near the center of the array.

Figure 2: Plot of the amplitude of the impedance matrix for the transmit array in cases of weak coupling (left) and strong coupling (right).

Figure 3: Self impedance (top row), average B_1^+ magnitude in the ROI, indicated by the blue circle, with 1 Ampere in each element driven separately (middle row) and optimal current amplitudes scaled to produce the fields shown in Table 1 (bottom row) for an ROI near the heart (left column) and ROI near the arm (left column) in the case where mutual coupling between elements is negligible.

Figure 4: Spatial distribution of the magnetic field $|B_1^+|$ obtained with the transmit array having weakly coupled elements driven in the three compared configurations. For each location of interest (indicated with a black circle), the three $|B_1^+|$ field distributions have been normalized to generate a whole-body average SAR equal to 2 W/kg.

Figure 5: Spatial distribution of the magnetic field $|B_1^+|$ obtained with the transmit array having strongly coupled elements driven in the three compared configurations. For each location of interest (indicated with a black circle), the three $|B_1^+|$ field distributions have been normalized to generate a whole-body average SAR equal to 2 W/kg.
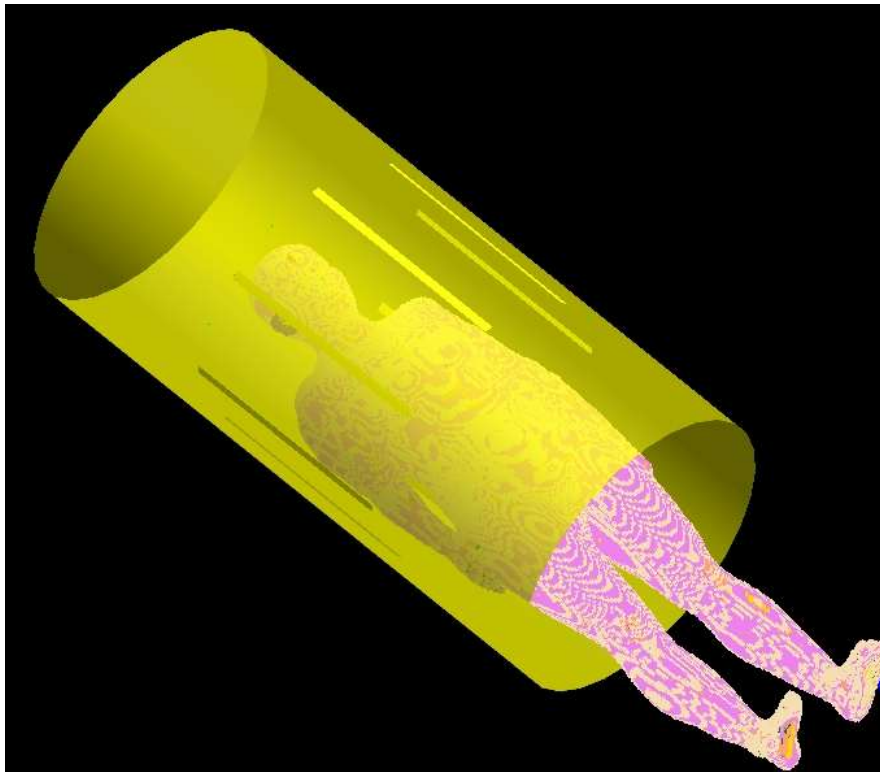
Figure 1: Geometry of the model used in simulations: a body-sized 8-element array of stripline elements spaced equidistantly on the surface of a cylinder within a large cylindrical shield and loaded with a human body model positioned with its heart near the center of the array.
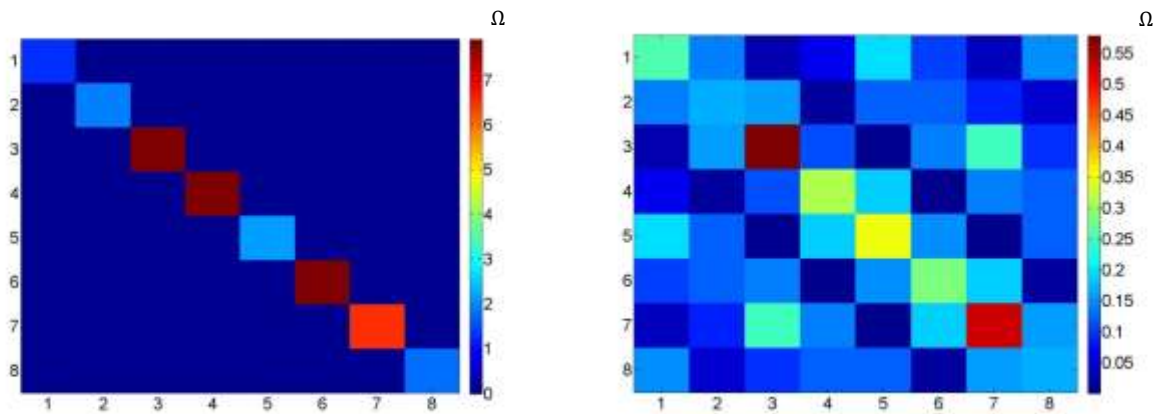

Figure 2: Plot of the amplitude of the impedance matrix of the transmit array in case of weak coupling (left) and strong coupling (right).
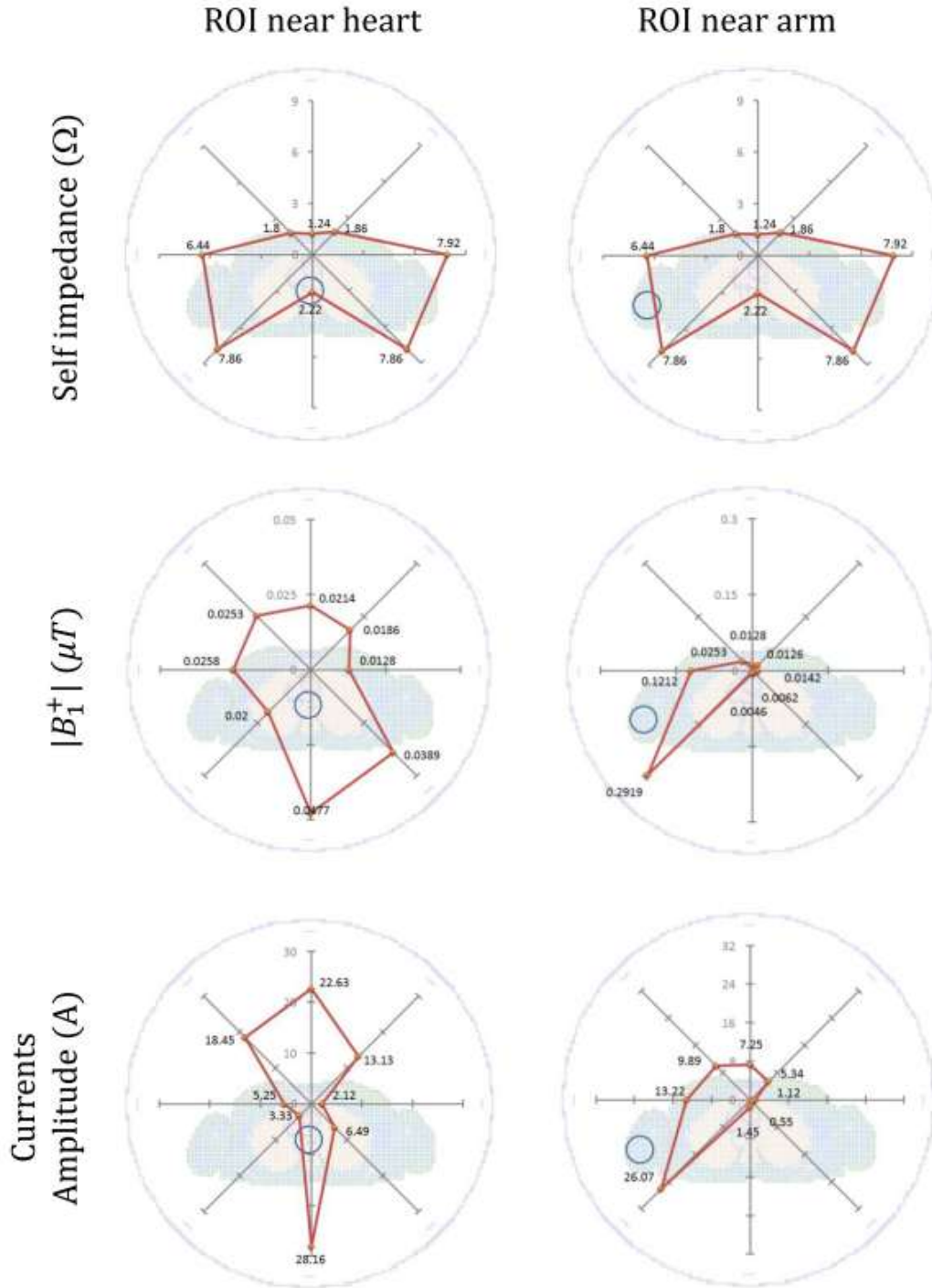
Figure 3: Graphical representation of the "Optimization with phase and amplitude" case reported in Table I. For each element of the array having negligible mutual coupling are provided the following. First row: values of the real part of the self-impedance $Re\{Z_{ii}\}$ (Ω); second row: average absolute values of the circularly polarized magnetic field in the two ROI , indicated by the blue circle; and, third row, amplitudes of the currents scaled to produce the fields shown in Table 1.
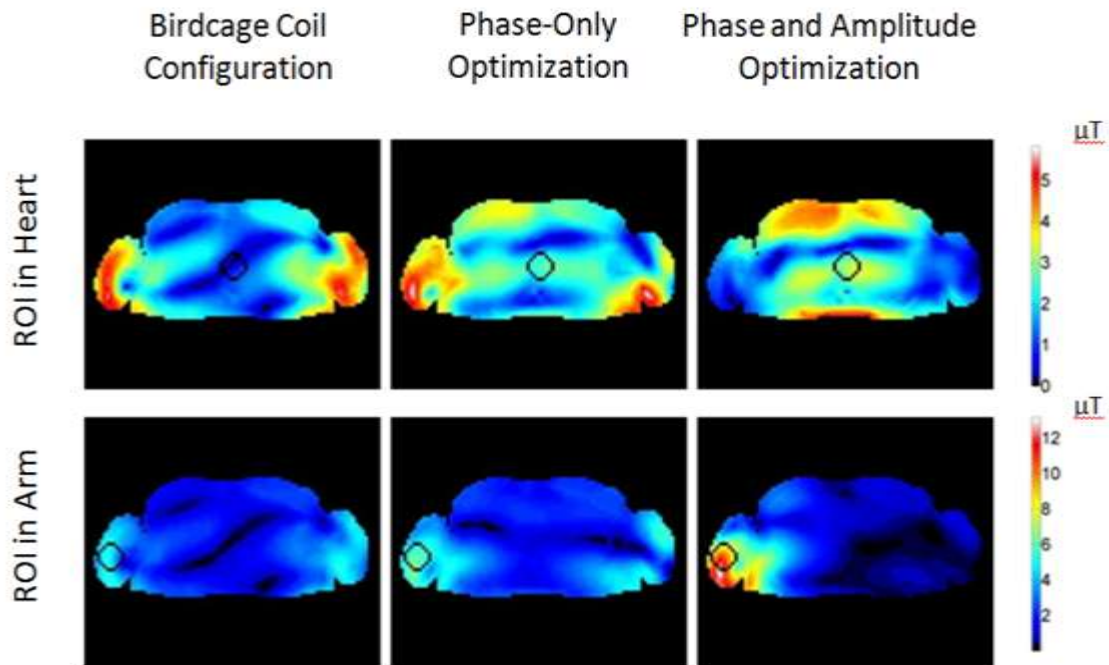
Figure 4: Spatial distribution of the magnetic field $|B_1^+|$ obtained with the transmit array having weakly coupled elements driven in the three compared configurations. For each location of interest (indicated with a black circle), the three $|B_1^+|$ field distributions have been normalized to generate a whole-body average SAR equal to 2 W/kg.
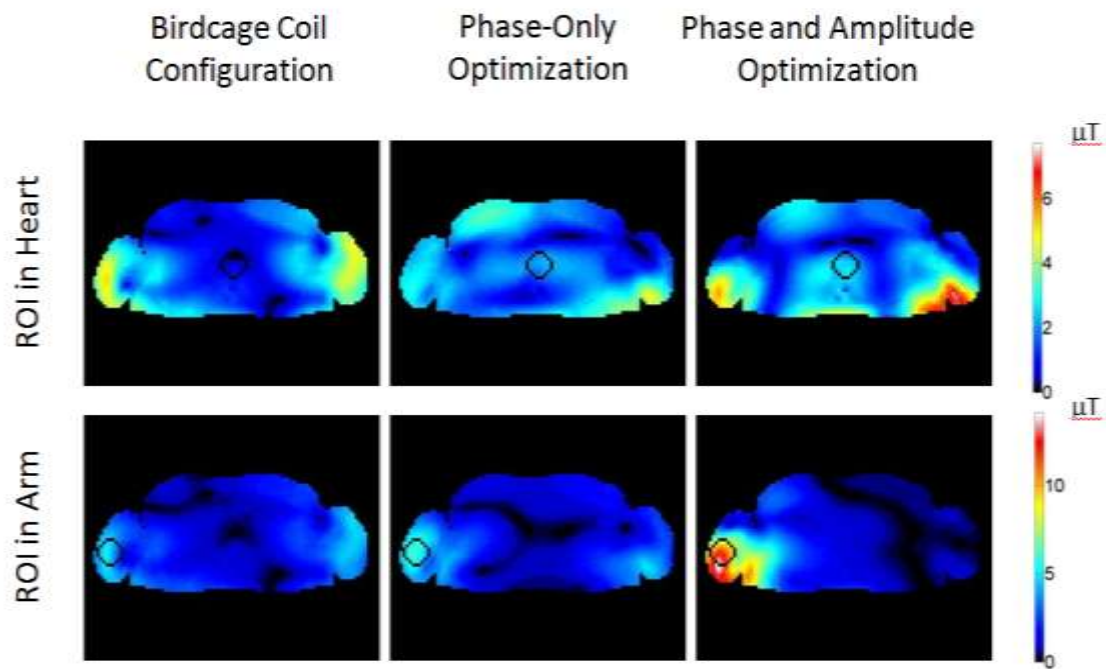
Figure 5: Spatial distribution of the magnetic field $|B_1^+|$ obtained with the transmit array having strongly coupled elements driven in the three compared configurations. For each location of interest (indicated with a black circle), the three $|B_1^+|$ field distributions have been normalized to generate a whole-body average SAR equal to 2 W/kg.